Multi-Scale Modeling of Phase Separation in Mixed Lipid Bilayers

Qiang Shi and Gregory A. Voth

Center for Biophysical Modeling and Simulation and Department of Chemistry, University of Utah, Salt Lake City, Utah

ABSTRACT   An approach to bridging the phenomenological field theory description of phase separation in binary mixed lipid bilayers with coarse-grained (CG) molecular dynamics (MD) simulation is presented. CG MD simulation is carried out for a 1:1 dipalmitoylphosphatidylcholine/dipalmitoylphosphatidylethanolamine lipid mixture at the liquid-gel phase coexistence condition. The liquid-gel phase separation can be characterized by the bilayer thickness, area per lipid molecule, and orientation parameter of the lipid tails. After a local order parameter is defined using the lipid tail bond orientation parameter, the CG MD data are bridged to a mesoscopic model based on the phenomenological Landau-Ginzberg free-energy functional. All parameters in this mesoscopic model are defined from the information of the phase boundary structure and the distributions of the order parameter in the liquid and gel phases. It is found that the mesoscopic model reproduces the equilibrium properties of the system very well, including collective fluctuations in both phases, spatial correlation functions of the order parameter, and the line tension. The possibility of using a time-dependent Landau-Ginzberg model to mimic the phase-separation dynamics is also investigated, using the relaxation time constant obtained by fitting the time-dependent correlation functions of the order parameter.

INTRODUCTION

The lipid bilayer that forms cell membranes is a two-dimensional liquid, whose structural and dynamic properties are of particular importance for the functioning of the cell (1). The traditional view of the lipid bilayer is of a two-dimensional homogeneous liquid that provides a barrier for the cell as well as a unique solvent for other functional units such as proteins. In recent years there is increasing evidence that cell membranes contain phase-separated domains of different lipid compositions called lipid rafts, which are believed to play an important role in many cell processes (for recent reviews, see (2–4)). The nature of the phase separation in real cell membranes is complicated due to the fact that many different kinds of proteins and lipid molecules may be involved. On the other hand, the characterization of phase-separation behavior in model membranes consisting of binary or ternary lipid mixtures has been more fruitful. It has been found experimentally that bilayers consisting of binary lipid mixtures show a liquid-gel phase separation (5–7), whereas ternary lipid mixtures consisting of saturated and unsaturated lipid, as well as cholesterol, exhibit liquid-liquid immiscibility and segregate into ordered (the liquid-ordered phase, l_o) and disordered (the liquid-disordered phase, l_d) phases under certain conditions (8–10).

Computer simulations play an increasingly important role in understanding biomembrane structure and dynamics. Molecular dynamics (MD) simulations using full atomistic models provide the most detailed information (see, e.g., (11–13) for recent reviews). Properties of binary and ternary mixed lipid bilayers have been studied using full atomistic simulations (14–18). However, the study of domain formation and phase separation using fully atomistic models is limited by the length- and timescales that can be reached by current computational methods. To make simulations at larger length- and timescales possible, a variety of coarse-grained (CG) models, where small groups of atoms are represented by a single interaction site, have been constructed. These include lattice models (6,19,20), off-lattice MD models (21–26), and models based on dissipative particle dynamics (27–29).

At even larger lengthscales (micrometers), the coarse-grained models also become computationally prohibitive. As such, an alternative scheme employs phenomenological models to describe the system at large lengthscales. A good example is the Helfrich Hamiltonian (30), which has been used successfully to predict cell shape and membrane conformation (31). For phase separation in mixed lipid bilayers, the most commonly used model is based on the Landau free energy (32). The Landau free energy model and Helfrich Hamiltonian have also been coupled together to study the shape deformation of vesicles resulting from intramembrane phase separation (33–35). In an even more general approach (36,37), various parameters are assigned from experimental and MD simulation data, which can be regarded as the first step to simulating phase separation coupled to membrane undulation dynamics in a realistic system.

To improve the predictive capability of computer simulations using the above mentioned hierarchy of theoretical models of lipid bilayers, an important goal is to build the multi-scale linkages between the coarse-grained models using simulation data from the more detailed ones. For example, full atomistic simulation data have been used to construct the CG models (23,25,26). Recently, MD and CG MD simulations have also been used to calculate the bending modulus in the Helfrich Hamiltonian (38–41). The goal of the present study is

to demonstrate an accurate yet practical procedure to bridge a phenomenological field theory model of phase separation to a CG model of a mixed lipid bilayer, and then to test its validity. For this purpose, CG MD simulation of a mixed dipalmitoylphosphatidylcholine/dipalmitoylphosphatidyletha-nolamine (DPPC/DPPE) bilayer is carried out at the liquid-gel phase coexistence condition, the parameters in the phenom-enological field theory model are then bridged, and, finally, equilibrium and dynamic properties predicted by this model are validated against the CG MD data. Since the current study is focused on the methodology to bridging a mesoscopic field theory model with a CG one, the requirement here of the CG model is to reproduce the basic physics, rather than to model the DPPC/DPPE mixed system accurately. The CG model accuracy is a topic of current research in our group, which will be addressed by utilizing our multi-scale coarse-graining method (26). Such an accurate CG model will be the topic of future publications.

MESOSCOPIC MODEL FOR PHASE-SEPARATION DYNAMICS

In the mesoscopic model, a local order parameter $\phi(\mathbf{x})$ describes the binary mixed bilayer under phase separation. The phase behavior of the binary mixture is determined by an effective Hamiltonian, in the form of a Landau free-energy functional:

$$F[\phi(\mathbf{x})] = \int d^{\mathrm{d}}\mathbf{x} \left[\frac{c}{2}|\nabla\phi(\mathbf{x})|^2 + f(\phi(\mathbf{x})) - \mu\phi(\mathbf{x}) \right]. \quad (1)$$

For a two-phase coexistence system, the free energy density $f(\phi)$ is of a double-well form, with the two minima giving stable phases at $\phi = \phi_1$ and $\phi = \phi_2$. The gradient term $c|\nabla\phi(\mathbf{x})|^2/2$ suppresses short-wave-length fluctuations of $\phi(\mathbf{x})$, and μ is the chemical potential. For simplicity, $f(\phi) - \mu\phi$ is combined into one term, $\tilde{f}(\phi)$, in the following discussions.

Phenomenological dynamics of the order parameter field $\phi(\mathbf{x})$ can be defined based on the effective Hamiltonian (Eq. 1). If the order parameter $\phi(\mathbf{x})$ is not a conserved variable, the Landau-Ginzberg model (or time-dependent Ginzberg-Landau equation) is usually used:

$$\frac{\partial\phi(\mathbf{x})}{\partial t} = -\Gamma\left(\frac{\delta F[\phi(\mathbf{x})]}{\delta\phi(\mathbf{x})}\right) + \zeta_{\mathrm{gl}}(\mathbf{x}, t). \quad (2)$$

The LG model gives pure dissipative dynamics. As in the Langevin equation for single particle motion, Gaussian noise $\zeta_{\mathrm{gl}}(\mathbf{x}, t)$ is introduced to ensure the correct fluctuation-dissipation relation. The correlation function of $\zeta_{\mathrm{gl}}(\mathbf{x}, t)$ is assumed to be

$$\langle\zeta_{\mathrm{gl}}(\mathbf{x}, t)\zeta_{\mathrm{gl}}(\mathbf{x}', t')\rangle = 2\Gamma k_{\mathrm{B}}T\delta(\mathbf{x} - \mathbf{x}')\delta(t - t'). \quad (3)$$

If $\phi(\mathbf{x})$ is a locally conserved variable, the Cahn-Hillard model (42) should be used,

$$\frac{\partial\phi(\mathbf{x})}{\partial t} = \lambda\nabla^2\left(\frac{\delta F[\phi(\mathbf{x})]}{\delta\phi(\mathbf{x})}\right) + \zeta_{\mathrm{ch}}(\mathbf{x}, t), \quad (4)$$

with correlation function for the Gaussian noise $\zeta_{\mathrm{ch}}(\mathbf{x}, t)$,

$$\langle\zeta_{\mathrm{ch}}(\mathbf{x}, t)\zeta_{\mathrm{ch}}(\mathbf{x}', t')\rangle = -2\lambda k_{\mathrm{B}}T\nabla^2\delta(\mathbf{x} - \mathbf{x}')\delta(t - t'). \quad (5)$$

COARSE-GRAINED MD SIMULATION OF MIXED LIPID BILAYER

For simplicity, the coarse-grained lipid model of Marrink et al. (24) is used in the present CG MD simulation. In this model, typically 4–6 heavy atoms are grouped into one interaction site. These interaction sites are further classified into four main types (polar, nonpolar, apolar, and charged) and 10 subtypes. Harmonic bond stretching and bending potentials are included as bonded interactions. All the non-bonded site potentials are short-ranged: a screened Coulomb potential with a cutoff is introduced to describe the interac-tion between the ionic headgroups; five different LJ potentials are used to describe the interactions between different sub-types of sites, mimicking interactions from hydrophobic to hy-drophilic, and in between. The model was parameterized using structural, dynamic, and elastic properties of a variety of phos-pholipids, and was found to reproduce these properties semi-quantitatively. This CG lipid model has also been shown to be able to capture the phase behavior of lipid bilayer self-assembly (24,43), and has been used to study the domain formation in DLPC/DSPC mixtures (44). In the future, our recently devel-oped multi-scale CG model (26) will be used for this purpose.

The CG MD simulation was carried out for a 1:1 DPPC/DPPE mixture using the GROMACS package (45,46) with the CG force field given in Marrink et al. (24) and at http://md.chem.rug.nl/~marrink/coarsegrain.html. The coarse-grained DPPC and DPPE molecules both have two sites for the headgroups, two sites representing the glycerol ester groups, and eight sites representing the two lipid tails (four sites each). The system consists of 1024 DPPC molecules and 1024 DPPE molecules, with each leaflet of the bilayer containing the same number of DPPC and DPPE molecules. A total of 30,720 coarse-grained water molecules were used as solvent. The simulation box was $23 \times 23 \times 12$ nm^3 in size, with the bilayer normal in the z direction. The system temperature and pressure were controlled using a weak coupling scheme (47). The semi-isotropic coupling with a pressure of 1 bar was chosen to mimic the zero surface tension condition, and the box compressibility was set to 5×10^{-6} bar^{-1}. The coupling time constant for the pressure and temperature control was 1 ps^{-1}, while the CG MD simulation time step was 40 fs.

The simulation was first carried out at different temper-atures to search for the phase coexistence region. Since this study is focused on how to map out the parameters of the mesoscopic model (Eq. 1) from a microscopic one, rather than the characterization of the phase diagram of the mixed bilayer system, one long simulation was carried out at 308 K where phase coexistence is clearly observed. It should be

noted that 308 K is not in the experimentally observed phase coexistence temperature range of ~315–333 K (48). This is due to the inaccuracy of the CG model we have employed here, which is only able to reproduce the physical property of real systems semiquantitatively (24). The total simulation time was 480 ns, which corresponds to 1.92-μs effective time, since the simulation time should be multiplied by a factor of 4 to account for the accelerated dynamical sampling in the CG model (Marrink et al. (24); note that effective times will be used throughout the following discussions). The last 1.28 μs of the trajectory was used for further analysis.

SIMULATION RESULTS

A snapshot of the mixed lipid bilayer showing phase separation is given in Fig. 1. To make the phase separation more visible, only one leaflet of the mixed bilayer is shown in the top view (Fig. 1 b). The liquid- and solidlike phase coexistence is seen clearly, with the liquid phase in the middle having a decreased thickness and the lipid tails more disordered.

Structures in the two phases can also be further characterized. The bilayer thickness D is defined as the difference of z coordinates between the center of mass of the first four CG sites (two head sites and two glycerol ester sites) of the lipid molecules in the upper and lower leaflets. Another important property characterizing the bilayer structure is the degree of order of the lipid carbon tails. The C-C (C stands for the CG sites of the lipid tails) bond orientation parameter S_z used in this study is defined as

$$S_z = \frac{1}{2N_{CC}} \sum_i (3\cos^2\theta_i - 1), \qquad (6)$$

where θ_i is the angle between the ith C-C bond and the bilayer normal, and N_{CC} is the total number of C-C bonds in the two lipid tails. The sum is carried out over all the C-C bonds.
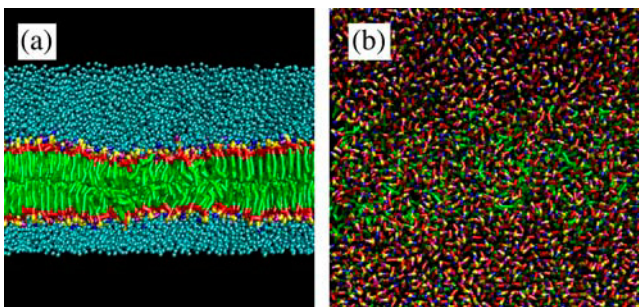
Since two phases are apparent, the mixed lipid bilayer was divided into liquid, solidlike, and boundary regions. The bilayer thickness D, area per lipid A, and orientation parameter S_z were calculated for the liquid and solidlike regions. They were found to be $D = 3.9$ nm, $A = 0.58$ nm^2, and $S_z = 0.50$ for the liquid phase; $D = 4.5$ nm, $A = 0.47$ nm^2, and $S_z = 0.89$ for the solidlike phase. To make a better assignment of the solidlike phase, diffusion constants were calculated in each phase by averaging the mean-square displacement over 20 CG molecules (Fig. 2). They were found to be $D_{liq} = 0.032$ nm^2/ns for the liquid phase and $D_{sol} = 0.0014$ nm^2/ns for the solidlike phase. The diffusion constant in the solidlike phase is large enough to suggest that it is not a crystal, and since it is more than an order-of-magnitude smaller than that in the liquid phase, it is also not the liquid-ordered phase that is often observed in systems containing cholesterol. The phase separation observed is thus a liquid-gel phase separation which should be observed for binary mixed lipid bilayer. This is also consistent with the findings in the DLPC/DSPC system using the same CG lipid model (44), where a liquid-gel phase separation was observed.

An interesting question is whether the liquid-gel phase separation is also accompanied by a composition separation of the two kinds of lipids. The x,y plane of the simulation box was divided into an 11×11 array of cells, and distributions of the two kinds of lipid molecules in the cells were calculated. The distributions of number difference $N_{PC} - N_{PE}$ is plotted in Fig. 3 for the liquid phase and gel phase. The two different kinds of lipid molecules were found to mix rather well. Part of the reason could be that the DPPC and DPPE molecules in the CG lipid model are quite similar; they are different only in one head site, with a slightly more attractive interaction between the DPPE-DPPE head sites than the DPPC-DPPC ones. It was also found that the liquid phase contains slightly more DPPC molecules, whereas the gel phase contains slightly more DPPE molecules—consistent with the fact that the DPPC
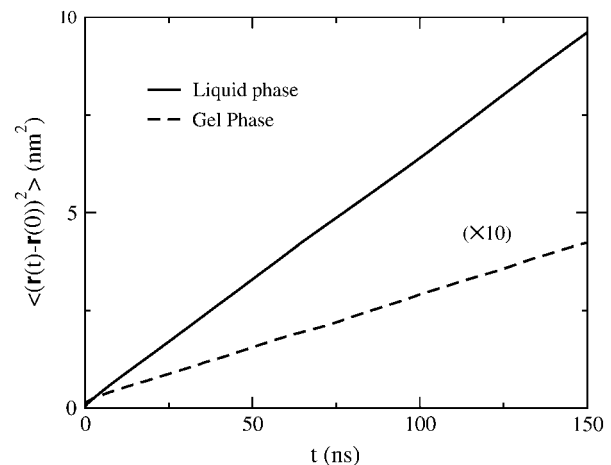

FIGURE 1 Snapshot of the mixed lipid bilayer showing phase co-existence. The headgroups are blue for DPPC, purple for DPPE, yellow for the PO$_4$ groups, red for the glycerol ester groups, green for the carbon tails, and cyan for CG water molecules; a is the side view, and b is the top view, where only one leaflet of the bilayer is shown to give a more clear view of the phase separation.

FIGURE 2 Mean-square displacements of lipid molecules in the liquid (*solid line*) and gel (*dashed line*, enlarged 10 times) regions calculated by averaging over 20 CG molecules in each phase.
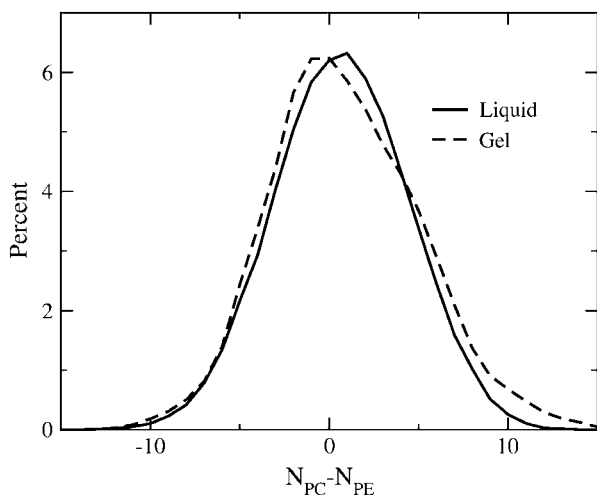
FIGURE 3 Distributions of the number difference, $N_{PC} - N_{PE}$, calculated on an area size of 2.08 nm × 2.08 nm for the liquid phase (*solid line*) and gel phase (*dashed line*).

bilayer has a lower melting temperature than the DPPE bilayer. A small degree of asymmetry in the number difference distribution was also observed in the gel phase.

MESOSCOPIC MODEL: PARAMETERS

To obtain the parameters in the mesoscopic model (Eq. 1) from CG MD simulation, an order parameter field $\phi(\mathbf{x})$ has to first be defined. Since there are quite obvious differences in the bilayer thickness D, area per lipid A, and tail C-C bond orientation parameter S_z between the liquid and gel phases, any local definition of these properties could be chosen as an order parameter. In contrast, although the composition difference is observed in the two phases, the difference is rather small, making it not as good a candidate for an order parameter. In the current study, the order parameter $\phi(\mathbf{x})$ is defined using S_z. However, other properties such as bilayer thickness D can be used as well to describe the same underlying physics of the phase separation, and the following bridging procedure is still valid. The specific choice of the order parameter for the mesoscopic field theory representation can also be dictated by the observable properties one may wish to subsequently calculate.

An order parameter S'_z is first defined based on a simple transformation of the S_z parameter. The reason for this is that if S_z has been used to define $\phi(\mathbf{x})$, the two phases would have quite different amplitude of fluctuations of the order parameter, but the fluctuations are found to have comparable spatial correlation length. This is not compatible with the simplest form of the effective Hamiltonian (Eq. 1). To solve this problem, a new parameter S'_z transformed from S_z is used to define $\phi(\mathbf{x})$. Details on why and how this transformation is made are elaborated in the Appendix. The transformation between S'_z and S_z used in this study is $S'_z = 0.73/(1.23 - S_z)$.

Since the order parameter S'_z is defined for a single molecule, a coarse-graining of the CG MD data is needed to calculate the local order parameter $\phi(\mathbf{x})$. As such, $\phi(\mathbf{x})$ is defined as the average of S'_z over all the lipid molecules in a rectangular box with the size $L \times L$, centered at $\mathbf{x}$ in the x,y plane of the mixed lipid bilayer. It should be noted that the coarse-graining box length L is an important parameter in the mesoscopic model, Eq. 1. All the parameters in this equation depend implicitly on L. The choice of L is based on the criteria that it should be much smaller than the dimensions of simulation box and, at the same time, much bigger than the size of a single lipid molecule. Different choices of L within these criteria give similar results and do not require changes in the following fitting procedure. In the current study, L is set to be 2.08 nm. Fig. 4 shows the order parameter field $\phi(\mathbf{x})$ calculated from a snapshot of the CG MD simulation. The lower $\phi(\mathbf{x})$ value region (*green*, more disordered) in the middle represents the liquid phase.

To get the free energy density $\tilde{f}(\phi)$, one key piece of information obtained from the CG MD simulation is the phase boundary structure, which describes the order parameter distribution at the boundary of the two coexisting phases. For example, when the phase coexistence system is assumed to be homogeneous in the x direction, the kink structure of the phase boundary is referred to the solution of $\phi(y)$ with boundary conditions $\phi = \phi_1$ at $y = -\infty$ and $\phi = \phi_2$ at $y = \infty$. In the mesoscopic model Eq. 1, it can be obtained by minimizing the total free energy (32), which gives

$$y - y_0 = \pm \int_{\phi(y_0)}^{\phi(y)} \frac{d\phi}{(2\tilde{f}(\phi)/c)^{1/2}}. \tag{7}$$

By taking the derivative of the above equation, the free energy density $\tilde{f}(\phi)$ divided by the constant c can be obtained:
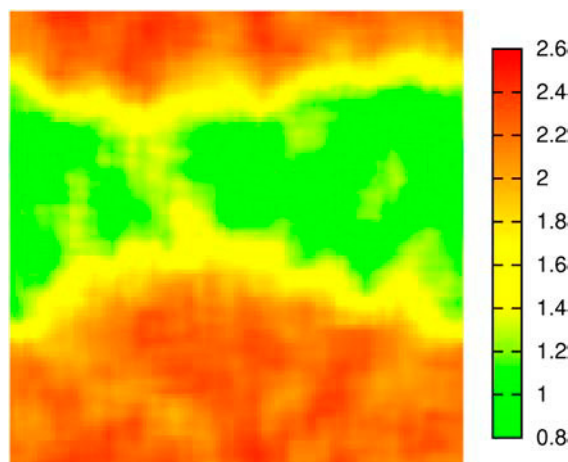

FIGURE 4 The order parameter field, $\phi(\mathbf{x})$, calculated from a snapshot of the CG MD simulation data.

$$\tilde{f}(\phi)/c = \frac{1}{2}\left(\frac{d\phi(y)}{dy}\right)^2. \qquad (8)$$

The following procedure is used to calculate the kink structure: first the boundary line between the liquid and gel phases is obtained, then, at selected points on this line, normals to the boundary are calculated. Coarse-grained order parameters $\phi(y)$ are calculated on points along the normals, where the absolute value of y is defined as the distance between these points and the boundary line, and the sign of y is defined as negative (−) for the liquid phase and positive (+) for the gel phase. As an example, $\phi(y)$ calculated using this method is shown in Fig. 5 (*circles*).

In the process to fit $\tilde{f}(\phi)/c$, it is found that the commonly used $\phi^2 - \phi^4$ form of the free energy density, i.e.,

$$\tilde{f}(\phi) = -\frac{r}{2}(\phi - \phi_0)^2 + u(\phi - \phi_0)^4, \qquad (9)$$

describes the simulation data rather well. Although this agreement could be a coincidence, the functional form Eq. 9 is used to fit the simulation data. Solution of the kink structure with the free energy density Eq. 9 is given by (32)

$$\phi(y) = \phi_0 \pm \phi_k \tanh[(y - y_0)/(\sqrt{2}\xi)], \qquad (10)$$

where $\xi = (c/r)^{1/2}$ is the correlation length, $\phi_k = (r/4u)^{1/2}$ defines the amplitude of the kink structure, and y_0 is the position where $\phi(y_0) = \phi_0$. The result of fitting the boundary structure using Eq. 10 is also given in Fig. 5 (*solid line*), which is in good agreement with the simulation result. The parameters obtained are $\xi = 0.98$ nm, $\phi_k = 0.58$, and $\phi_0 = 1.65$. The function $\tilde{f}(\phi)/c$ obtained from Eq. 9 (a constant shift is added to make $\tilde{f}(\phi) = 0$ at the two minima) is shown in Fig. 6 (*dashed line*), which agrees well with the result (*solid line* and *circles*) calculated using the numerical derivative of $\phi(y)$ (Eq. 8).
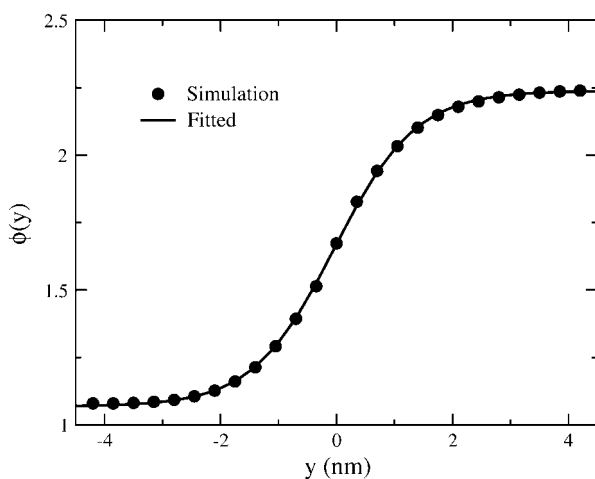

FIGURE 5   The phase boundary kink structure calculated from CG MD simulation (*circles*) and fitted using Eq. 10 (*solid line*).
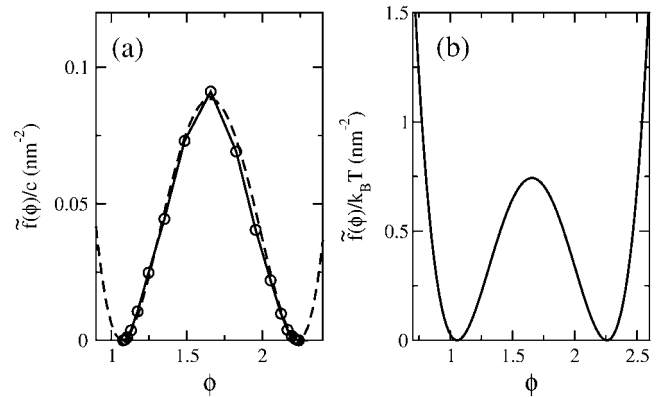

FIGURE 6   (*a*) The function $\tilde{f}(\phi)/c$ calculated by fitting the kink structure from the $\phi^2 - \phi^4$ model (*dashed line*) and from numerical derivative of $\phi(y)$ using Eq. 8 (*solid line* and *circles*). (*b*) The free energy density by combining $\tilde{f}(\phi)/c$ and the c constant obtained by matching the ϕ distributions to the CG MD data.

The above procedure only gives the shape of the free energy density $\tilde{f}(\phi)/c$. To get the absolute value of $\tilde{f}(\phi)$, the constant c has to be obtained. For this purpose, a 11×11 lattice model mimicking the mixed lipid bilayer in the CG MD simulation is constructed, and the LG dynamics is used to calculate the equilibrium distribution of ϕ from the Landau free energy (Eq. 1) around the liquid phase (ϕ_1) and gel phase (ϕ_2). (The equilibrium distributions are determined by the Landau free energy, not the details of the dynamics.) The distributions calculated from the Landau free energy model are then compared with the data obtained from CG MD simulation. The constant c is obtained by matching the lattice model distributions of ϕ and the same distributions from CG MD simulation.

It should be noted that Eqs. 7 and 8 are obtained by neglecting the thermal fluctuations. Since the free energy density (Eq. 9) is anharmonic, the kink structure calculated by averaging $\phi(\mathbf{x})$ along the normals to the phase boundary line should not be the same as those calculated by minimization of the total free energy. It is believed, however, that there should not be a qualitative difference. For example, in the quartic $\phi^2 - \phi^4$ model, the two most important parameters ϕ_k and ξ represent the amplitude of the kink structure and the correlation length (Eq. 10), and they should not be very different when calculated with or without thermal fluctuations. In fact, when the $\tilde{f}(\phi)/c$ fitted using Eq. 10 is used to calculate the distributions of $\phi(\mathbf{x})$, the maxima of the distributions are observed to be shifted by 2–3%, comparing to the CG MD result. Since the difference is quite small, the free energy density is simply stretched somewhat to fit the CG MD distributions. The c constant is found to be $c = 8.0$ k_BT, and the result of matching the mesoscopic model and CG MD distributions is shown in Fig. 7. It can be seen that the mesoscopic model reproduces the distributions of order parameter in both phases rather well.
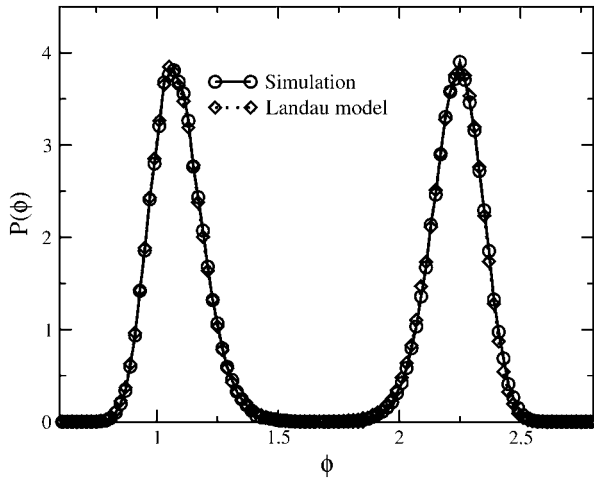
FIGURE 7 Distributions of the order parameter ϕ in the liquid (*left*) and gel (*right*) phases. The circles are from CG MD simulation, and the diamonds are from the fitted Landau free energy model.

In the above procedure, all the parameters in the effective Hamiltonian (Eq. 1) have been obtained from the phase boundary kink structure and distributions of order parameters in the liquid and gel phases. It is important now to test whether the Landau free energy model using the above fitted parameters can reproduce other equilibrium properties of the mixed bilayer system.

The first property used to test the validity of the mesoscopic model is the amplitude of collective fluctuations in the liquid and gel phases. The average of order parameter over an area A is defined as

$$\bar{\phi} = \frac{1}{A} \int d\mathbf{x}\phi(\mathbf{x}). \tag{11}$$

Assuming that the system lies closely to one of the two minima ϕ_1 (liquid phase) or ϕ_2 (gel phase), a first approximation is to expand the free energy density $\tilde{f}(\phi)$ near the minima to second order $\tilde{f}(\phi) \approx \tilde{f}(\phi_i) + 1/2\tilde{f}''(\phi_i)(\phi - \phi_i)^2$. This approximation gives a solvable Gaussian model, which predicts

$$\langle(\bar{\phi} - \phi_i)^2\rangle = \frac{k_B T}{A\tilde{f}''(\phi_i)}. \tag{12}$$

Using the above equation, we estimated the value $\tilde{f}''(\phi_i)$ from $\langle(\bar{\phi} - \phi_i)^2\rangle$, as calculated for the liquid and gel phases from CG MD data. They were found to be $\tilde{f}''(\phi_1) = 12.7\,k_B T/nm^2$ for the liquid phase and $\tilde{f}''(\phi_2) = 8.8\,k_B T /nm^2$ for the gel phase. The value given from the fitted free energy density is $16.7\,k_B T/nm^2$ for the two phases. The agreement is fair, and one source of error could be that Eq. 12 is derived for a one-phase system with periodic boundary conditions, whereas the values calculated using CG MD data are from a phase-coexistence system.

The spatial correlation functions of the order parameter $\phi(\mathbf{x})$ can also be calculated for the liquid and gel phases, and

compared with the result from the lattice model using the Landau free energy model. This is done by dividing the x,y plane of the mixed bilayer into a $N \times N$ grid and calculating the average $G(\mathbf{x} - \mathbf{x}') = \langle(\phi(\mathbf{x}) - \phi_i)(\phi(\mathbf{x}') - \phi_i)\rangle$ for the two phases, where the values ϕ_i ($i = 1$ for the liquid phase, $i = 2$ for the gel phase) are the two minima of $\tilde{f}(\phi)$. The value $N = 11$ was used in the current study, since if the correlation functions are calculated on a finer grid, the spacing between neighboring grid points will be smaller than the coarse-graining box length L used to calculate the local order parameter, and thus some artificial correlations will be introduced. The results from the CG MD simulation and the Landau free energy model are shown in Fig. 8. It can be seen there that the prediction of the Landau free energy model agrees well with the CG MD result.

Another important property of the phase coexistence system is the line tension σ, which can also be estimated from the simulation data. The distribution $P(l_b)$ of the boundary line length l_b is first calculated and the following equation is used to fit the distribution:

$$P(l_b) \propto P_0(l_b)e^{-\sigma l_b/k_B T}. \tag{13}$$

In the above equation, σ is the line tension and $P_0(l_b)$ is the density of states of l_b. The form of $P_0(l_b)$ is assumed to be $P_0(l_b) \propto (l_b - l_0)^n$ when $l_b \geq l_0$, and $P_0(l_b) = 0$ when $l_b < l_0$, where l_0 is the box length along the x direction. The function $P(l_b)$ (*circles*) and the fitted result using Eq. 13 (*solid line*) are shown in Fig. 9. The best fitting is obtained when $n = 2$, and the line tension is found to be $\sigma = 2.6\,k_B T/nm$. The line tension can also be calculated for the $\phi^2 - \phi^4$ model by (32)

$$\sigma = 2\sqrt{2}/3(\xi r\phi_k^2), \tag{14}$$

and is found to be $\sigma = 2.8\,k_B T/nm$, which agrees very well with the fitted result.

After the validity of the mesoscopic model in reproducing the equilibrium properties is established, another important
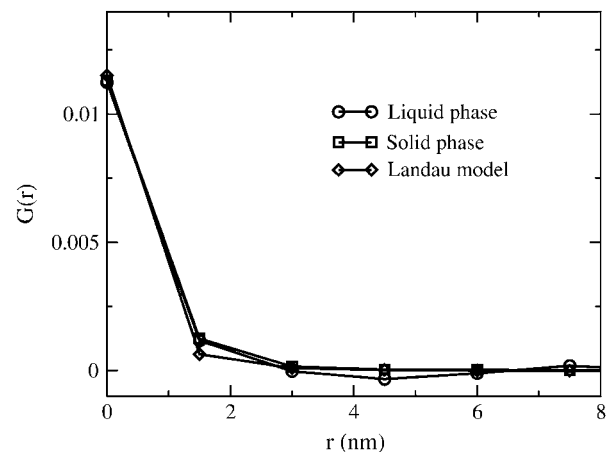

FIGURE 8 Spatial correlation function of ϕ calculated for the liquid (*circles*) and gel (*squares*) phases from CG MD data, and from the fitted Landau free energy model (*diamonds*).
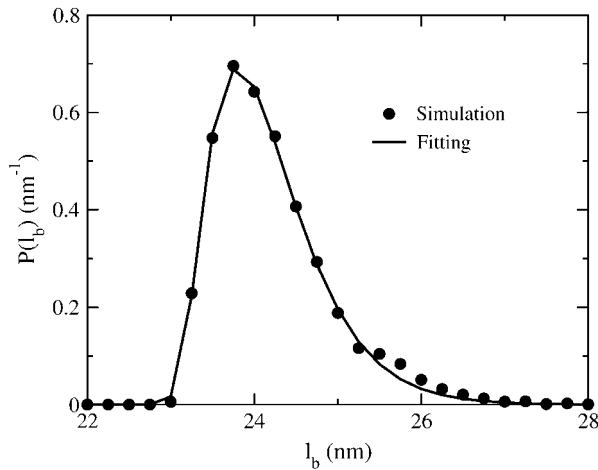
FIGURE 9 The distribution of the length of phase boundary lines calculated from CG MD data (*circles*) and fitted using Eq. 13 (*solid line*).

FIGURE 10 Time-dependent correlation function $C(t)$ (normalized to $C(0)$) of the order parameter $\phi(\mathbf{x})$. (*a*) CG MD result for the liquid (*circles*) phase and gel (*squares*) phase, fitted using a sum of three exponentials (*solid lines*). (*b*) LG dynamics result (*diamonds*) and a one-exponential fit (*solid line*).

question is whether the LG dynamics can capture the phase-separation dynamics of the CG MD model (since $\phi(\mathbf{x})$ is not a conserved variable, the LG dynamics is more appropriate than the CH dynamics). The time-dependent correlation functions of the order parameter $C(t) = \langle (\phi(\mathbf{x}, t) - \phi_i)(\phi(\mathbf{x}, 0) - \phi_i) \rangle$ (where $\phi(\mathbf{x}, t)$ is the coarse-grained local order parameter at time t, and the ϕ_i values are the minima of $\tilde{f}(\phi)$ for the liquid phase ($i = 1$) and the gel phase ($i = 2$)) are calculated for each of the phases, and are shown in Fig. 10 a.

The same correlation function can be calculated using LG dynamics, i.e.,

$$\frac{\partial \phi(\mathbf{x}, t)}{\partial t} = \Gamma c \nabla^2 \phi(\mathbf{x}, t) - \Gamma \tilde{f}'[\phi(\mathbf{x}, t)] + \zeta_{gl}(\mathbf{x}, t). \quad (15)$$

As can be seen in the calculation of the spatial correlation functions (Fig. 8), because the correlation length is smaller than the lattice size, the gradient term in the above equation can thus be neglected as a first approximation. When the Gaussian approximation is also applied, Eq. 15 can be simplified to give

$$\frac{\partial [\phi(\mathbf{x}, t) - \phi_i]}{\partial t} \approx -\Gamma \tilde{f}''(\phi_i)[\phi(\mathbf{x}, t) - \phi_i] + \zeta_{gl}(\mathbf{x}, t). \quad (16)$$

The LG dynamics then yields an exponential decay of the correlation function,

$$C(t)/C(0) = \exp[-\Gamma \tilde{f}''(\phi_i)t]. \quad (17)$$

The numerical result of the LG correlation function is shown in Fig. 10 b. As can be seen from the plots, a single exponential fits the correlation function rather well. Using the approximation from Eq. 17, the second-order derivative $\tilde{f}''(\phi_i)$ is estimated to be 19.3 k_BT/nm^2, which is close to the value $\tilde{f}''(\phi_i) = 16.7 k_BT/nm^2$ used in the LG simulation.

It is obvious from Fig. 10 a that the CG MD correlation functions show a multi-timescale behavior, and this is of no surprise since different kinds of molecular motion are likely
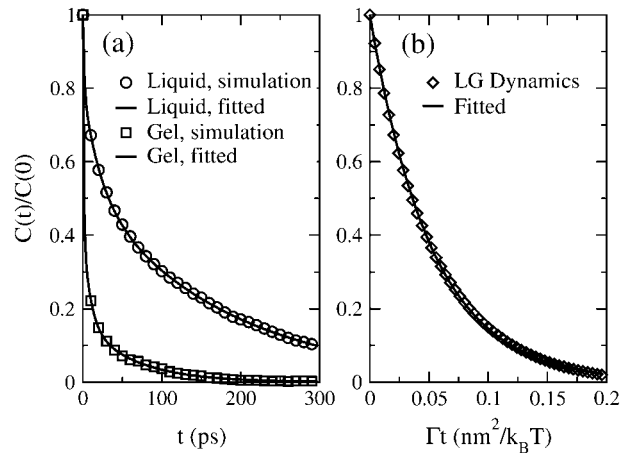
involved, e.g., the fast timescales would come from vibrational and rotational motions. Both correlation functions are fitted using a sum of three exponentials, with the results of the fitting given in Table 1.

When the LG dynamics are used to mimic the CG MD phase-separation dynamics, the slowest timescale obtained from the above three-exponential fitting is used to match the LG dynamics correlation function, which gives the relaxation constant $\Gamma = 0.28$ (nm^2/k_BT)ns^{-1} (the slowest timescale for the liquid phase, 5.5 ns^{-1}, is used). The question then is whether the LG model can represent the phase-separation dynamics well. To test this, the diffusive motion of the phase boundary is calculated. In the current simulation, the phase boundary moves randomly in the y-direction—which, in the long time limit, shows a diffusive behavior. It should be noted that this diffusive motion of the phase boundary line is a result of collective motion of the system and is quite different from the diffusion of individual lipid molecules. The diffusion constant of such motion is calculated from the mean-square displacement of the average value of the y coordinate of the phase boundary line (y_c), which is found to be $D' = 0.01$ nm^2/ns from CG MD simulation (Fig. 11). The result from LG dynamics

TABLE 1 Three-exponential fitting of the (normalized) time-dependent correlation function of the order parameter: $C(t)/C(0) = \sum_{i=1}^{3} c_i e^{-\gamma_i t}$

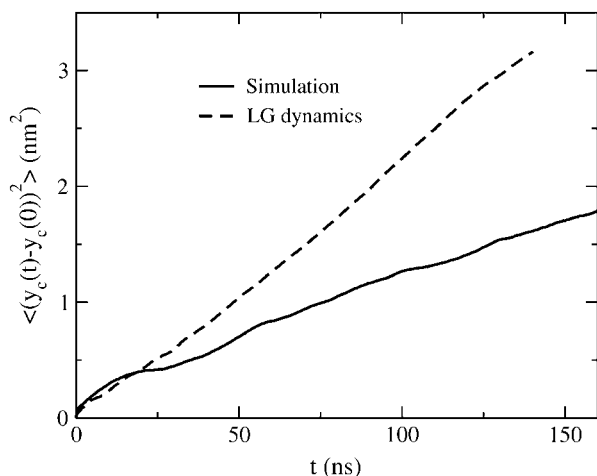|	c_i	γ_i(ns^{-1})
Liquid phase	0.20	630
	0.27	47
	0.53	5.5
Gel phase	0.58	1000
	0.26	110
	0.16	16

FIGURE 11 The mean-square displacements of average *y* coordinate of the phase boundary line, calculated from CG MD simulation (*solid line*), and LG dynamics (*dashed line*).

simulation is also shown in Fig. 11 (*dashed line*), using the relaxation constant Γ obtained above. The diffusion constant is found to be $D' = 0.02$ nm^2/ns, which is at least of the same order of magnitude as the result from CG MD simulation. The LG dynamics can therefore capture some aspects of the CG MD phase-separation dynamics without further theoretical improvements, which are in progress.

DISCUSSION AND CONCLUSIONS

In this article, a mesoscopic model based on the Landau-Ginzberg free energy theory was constructed to characterize the liquid-gel phase separation of binary mixed lipid bilayers. The parameters in the mesoscopic model are bridged in a multi-scale fashion from CG MD simulation data. It is found that the mesoscopic model reproduces the equilibrium properties of the liquid-gel phase-separation system quite well. An implication from this result is that when only equilibrium properties are considered, or when there is a separation of timescales where the phase-separation dynamics reaches equilibrium faster than other dynamical variables, the mesoscopic model using a Landau-Ginzberg free energy theory can be very useful. Although the phenomenological dynamics using the LG dynamics is not quite able to capture the multi-timescale motion of the order parameter field, it is able to reproduce some slow motion behavior of the phase-separation dynamics such as the phase boundary diffusive motion. This result is also encouraging since the long timescale dynamics is usually more important to model large lengthscale objects such as vesicles. Further work along these lines, and to improve the accuracy of the mesoscopic dynamical model, is in progress.

The main goal of this article was to find a practical multi-scale approach for bridging a mesoscopic model of phase separation in mixed lipid bilayers with a more detailed

microscopic model. The mapping procedure used in this study can be extended in several ways. First, it would be interesting to apply the current approach to ternary mixed lipid bilayers, where the liquid-liquid immiscibility is more closely related to the behavior of real biological membranes and the phenomenological dynamics should be different as well (e.g., CH dynamics instead of LG dynamics). Second, in real systems such as giant unilamellar vesicles and biological membranes, the phase-separation dynamics would not likely act alone but rather be coupled to other types of long timescale dynamics. These include the long wavelength undulation motions of the lipid bilayer and hydrodynamic motions of both the lipid bilayer and the environment. The correct representation of these couplings seems critical for a mesoscopic model to simulate complex processes of real membranes such as budding. The possibility of multi-scale bridging to these different kinds of motion from a CG MD model could also be investigated by extending the approach used in this study, and such work is presently underway in our group.

APPENDIX: TRANSFORMATION BETWEEN S'_z AND S_z

In a Gaussian approximation to the effective Hamiltonian (Eq. 1), the correlation length and equilibrium fluctuation amplitude are determined by the two parameters $\tilde{f}''(\phi_0)$ (second-order derivative of $\tilde{f}(\phi)$ at the minimum of the free energy density ϕ_0) and c. It is found that if S_z is used to define the order parameter $\phi(\mathbf{x})$, there will be similar correlation lengths, but quite different amplitudes for the fluctuations of $\phi(\mathbf{x})$ in the liquid and gel phases. So if the constant c is the same for the two phases, based on their similar correlation lengths, they should have similar values of $\tilde{f}''(\phi_0)$; however, based on the amplitudes of the fluctuations, $\tilde{f}''(\phi_0)$ should be very different in the two phases. One solution to this problem is to use a ϕ-dependent c parameter in Eq. 1, which will make the free energy functional more complicated; the other is to do a transformation from S_z to a new parameter S'_z, such that when S'_z is used to define $\phi(\mathbf{x})$, the fluctuation amplitudes in the liquid and gel phases will be roughly the same, and the simple form of Eq. 1 (i.e., keeping c as a constant) can be retained. The latter approach is used in this study.

There is no unique way to define the nonlinear transform function between S'_z and S_z. By noticing the fact that S_z is bounded, $-1/2 < S_z < 1$, the function used in this study is

$$S'_z = \frac{A}{B - S_z}. \qquad (18)$$

(Note that, in this case, $B > 1$ is used to enhance the fluctuations in the gel phase and, at the same time, suppress the fluctuations in the liquid phase.) Equation 18 is, in fact, one of the simplest functions that can be used to do the transform, since only one adjustable parameter B is involved (A can be selected arbitrarily). As stated above, B is chosen such that when S'_z is used to define $\phi(\mathbf{x})$, the fluctuations in the liquid and gel phases have roughly the same amplitude. It is found that $B = 1.23$ does the job well; $A = 0.73$ is then arbitrarily chosen to make the values of $\phi(\mathbf{x})$ in the liquid phase at ~1.0.

REFERENCES

1. Gennis, R. B. 1989. Biomembranes: Molecular Structure and Function. Springer-Verlag, New York.

2. Brown, D. A., and E. London. 1998. Functions of lipid rafts in biological membranes. *Annu. Rev. Cell Dev. Biol.* 14:111–136.

3. Edidin, M. 2003. The state of lipid rafts: from model membranes to cells. *Annu. Rev. Biophys. Biomol. Struct.* 32:257–283.

4. Simons, K., and W. L. C. Vaz. 2004. Model systems, lipid rafts, and cell membranes. *Annu. Rev. Biophys. Biomol. Struct.* 33:269–295.

5. Mabrey, S., and J. M. Sturtevant. 1976. Investigation of phase transitions of lipids and lipid mixtures by high sensitivity differential scanning calorimetry. *Proc. Natl. Acad. Sci. USA.* 73:3862–3866.

6. Jorgensen, K., A. Klinger, and R. L. Biltonen. 2000. Nonequilibrium lipid domain in the gel-fluid two-phase region of a $DC_{16}PC$-$DC_{12}PC$ lipid mixture investigated by Monte Carlo computer simulation, FT-IR, and fluorescence spectroscopy. *J. Phys. Chem. B.* 104:11763–11773.

7. Bagatolli, L. A., and E. Gratton. 2000. Two photon fluorescence microscopy of coexisting lipid domains in giant unilamellar vesicles of binary phospholipid mixtures. *Biophys. J.* 78:290–305.

8. Dietrich, C., L. Bagatolli, Z. N. Volovyk, N. L. Thompson, M. Levi, K. Jacobson, and L. A. Gratton. 2001. Lipid rafts reconstituted in model membranes. *Biophys. J.* 80:1417–1428.

9. Samsonov, A. V., I. Mihalyov, and F. S. Cohen. 2001. Characterization of cholesterol-sphingomyelin domains and their dynamics in bilayer membranes. *Biophys. J.* 81:1486–1500.

10. Veatch, S. L., and S. L. Keller. 2002. Lateral organization in lipid membranes containing cholesterol. *Phys. Rev. Lett.* 89:268101.

11. Tieleman, D. P., S. J. Marrink, and H. J. C. Berendsen. 1997. A computer perspective of membranes: molecular dynamics studies of lipid bilayer systems. *Biochim. Biophys. Acta.* 1331:235–270.

12. Forrest, L. R., and M. S. P. Sansom. 2000. Membrane simulations: bigger and better? *Curr. Opin. Struct. Biol.* 10:174–181.

13. Feller, S. E. 2000. Molecular dynamics simulation of lipid bilayers. *Curr. Opin. Colloid Interf. Sci.* 5:217–223.

14. Tu, K., M. L. Klein, and D. J. Tobias. 1998. Constant-pressure molecular dynamics investigation of cholesterol effects in a dipalmitoylphosphatidylcholine bilayer. *Biophys. J.* 75:2147–2156.

15. Smondyrev, A. M., and M. L. Berkowitz. 1999. Structure of dipalmitoylphosphatidylcholine/cholesterol bilayer at low and high cholesterol concentrations: molecular dynamics simulation. *Biophys. J.* 77:2075–2089.

16. Khelashvili, G., and H. L. Scott. 2004. Combined Monte Carlo and molecular dynamics simulation of hydrated 18:0 sphingomyelin-cholesterol lipid bilayers. *J. Chem. Phys.* 120:9841–9847.

17. de Vries, A. H., A. E. Mark, and S. J. Marrink. 2004. The binary mixing behavior of phospholipids in a bilayer: a molecular dynamics study. *J. Phys. Chem. B.* 108:2454–2463.

18. Pandit, S. A., E. Jakobsson, and H. L. Scott. 2004. Simulation of the early stages of nano-domain formation in mixed bilayers of sphingomyelin, cholesterol, and dioleoylphosphatidylcholine. *Biophys. J.* 87:3312–3322.

19. Jorgensen, K., and O. G. Mouritsen. 1995. Phase separation dynamics and lateral organization of two-component lipid membranes. *Biophys. J.* 69:942–954.

20. Michonova-Alexova, E. I., and I. P. Sugar. 2002. Component and state separation in DMPC/DSPC lipid bilayers: a Monte Carlo simulation study. *Biophys. J.* 83:1820–1833.

21. Smit, B., P. A. J. Hilbers, K. Esselink, L. A. M. Rupert, N. M. van Os, and A. G. Schlijper. 1990. Computer simulations of the water/oil interface in the presence of micelles. *Nature.* 348:624–625.

22. Goetz, R., and R. Lipowsky. 1998. Computer simulations of bilayer membranes: self-assembly and interfacial tension. *J. Chem. Phys.* 108:7397–7409.

23. Shelley, J. C., M. Y. Shelley, R. C. Reeder, S. Bandyopadhyay, and M. L. Klein. 2001. A coarse-grain model for phospholipid simulations. *J. Phys. Chem. B.* 105:4464–4470.

24. Marrink, S. J., A. H. de Vries, and A. E. Mark. 2004. Coarse-grained model for semiquantitive lipid simulations. *J. Phys. Chem. B.* 108:750–760.

25. Murtola, T., E. Falck, M. Patra, M. Karttunen, and I. Vattulainen. 2004. Coarse-grained model for phospholipid/cholesterol bilayer. *J. Chem. Phys.* 121:9156–9165.

26. Izvekov, S., and G. A. Voth. 2005. A multi-scale coarse-graining method for biomolecular systems. *J. Phys. Chem. B.* 109:2469–2473.

27. Venturoli, M., and B. Smit. 1999. Simulating the self-assembly of model membranes. *Phys. Chem. Comm.* 10:45–49.

28. Shillcock, J. C., and R. Lipowsky. 2002. Equilibrium structure and lateral stress distribution of amphiphilic bilayers from dissipative particle dynamics simulations. *J. Chem. Phys.* 117:5048–5061.

29. Groot, R. D., and K. L. Rabone. 2001. Mesoscopic simulation of cell membrane damage, morphology change and rupture by nonionic surfactants. *Biophys. J.* 81:725–736.

30. Helfrich, W. 1973. Elastic properties of lipid bilayers: theory and possible experiments. *Z. Naturforsch.* 28:693–703.

31. Lipowsky, R. 1991. The conformation of membranes. *Nature.* 349:475–481.

32. Chaikin, P. M., and T. C. Lubensky. 2000. Principles of Condensed Matter Physics. Cambridge University Press, Cambridge, UK.

33. Taniguchi, T. 1996. Shape deformation and phase separation dynamics of two-component vesicles. *Phys. Rev. Lett.* 76:4444–4447.

34. Kumar, P. B. S., and M. Rao. 1998. Shape instabilities in the dynamics of a two-component fluid membrane. *Phys. Rev. Lett.* 80:2489–2492.

35. Jiang, Y., T. Lookman, and A. Saxena. 2000. Phase separation and shape deformation of two-phase membranes. *Phys. Rev. E.* 61:R57–R60.

36. McWhirter, J. L., G. Ayton, and G. A. Voth. 2004. Coupling field theory with mesoscopic dynamical simulations of multicomponent lipid bilayers. *Biophys. J.* 87:3242–3263.

37. Ayton, G., J. L. McWhirter, P. McMurtry, and G. A. Voth. 2005. Coupling field theory with continuum mechanics: a simulation of domain formation in giant unilamellar vesicles. *Biophys. J.* 88:3855–3869.

38. Goetz, R., G. Gompper, and R. Lipowsky. 1999. Mobility and elasticity of self-assembled membranes. *Phys. Rev. Lett.* 82:221–224.

39. Lindahl, E., and O. Edholm. 2000. Mesoscopic undulations and thickness fluctuations in lipid bilayers from molecular dynamics simulations. *Biophys. J.* 79:426–433.

40. Marrink, S. J., and A. E. Mark. 2004a. Effect of undulations on surface tension in simulated bilayers. *J. Phys. Chem. B.* 105:6122–6127.

41. Ayton, G., and G. A. Voth. 2002. Bridging microscopic and mesoscopic simulations of lipid bilayers. *Biophys. J.* 83:3357–3370.

42. Cahn, J. W., and J. E. Hilliard. 1958. Free energy of a nonuniform system. I. Interfacial free energy. *J. Chem. Phys.* 28:258–267.

43. Marrink, S. J., and A. E. Mark. 2004b. Molecular view of hexagonal phase formation in phospholipid membranes. *Biophys. J.* 87:3894–3900.

44. Faller, R., and S. J. Marrink. 2004. Simulation of domain formation in DLPC-DSPC mixed bilayers. *Langmuir.* 20:7686–7693.

45. Berendsen, H. J. C., D. van der Spoel, and R. van Drunen. 1995. GROMACS: a message-passing parallel molecular dynamics implementation. *Comp. Phys. Comm.* 91:43–56.

46. Lindahl, E., B. Hess, and D. van der Spoel. 2001. GROMACS 3.0: a package for molecular simulation and trajectory analysis. *J. Mol. Modeling.* 7:306–317.

47. Berendsen, H. J. C., J. P. M. Postma, W. F. van Gunsterrn, A. DiNola, and J. R. Haak. 1984. Molecular dynamics with coupling to an external bath. *J. Chem. Phys.* 81:3684–3690.

48. Caffrey, M., and F. S. Hing. 1987. A temperature gradient method for lipid phase diagram construction using time-resolved x-ray diffraction. *Biophys. J.* 51:37–46.